Discovery of 4*H*-thieno[3,2-*b*]pyrrole derivatives as potential anticancer agents

Bo Fang[a,b], Chunsheng Hu[a,b], Yong Ding[a], Hongxia Qin[b], Yafei Luo[a], Zhigang Xu[a,b], Jiangping Meng[a,b], Zhongzhu Chen[a,b]

[a] National & Local Joint Engineering Research Center of Targeted and Innovative Therapeutics, College of Pharmacy & International Academy of Targeted Therapeutics and Innovation, Chongqing University of Arts and Sciences, Chongqing, China.

[b] Chongqing Engineering Laboratory of Targeted and Innovative Therapeutics, Chongqing Key Laboratory of Kinase Modulators as Innovative Medicine, Chongqing Collaborative Innovation Center of Targeted and Innovative Therapeutics, Chongqing University of Arts and Sciences, Chongqing, China.

Correspondence

Jiangping Meng, National & Local Joint Engineering Research Center of Targeted and Innovative Therapeutics, College of Pharmacy & International Academy of Targeted Therapeutics and Innovation, Chongqing University of Arts and Sciences, Chongqing, 402160, China. E-mail: mengjp2006@163.com

Zhongzhu Chen, National & Local Joint Engineering Research Center of Targeted and Innovative Therapeutics, College of Pharmacy & International Academy of Targeted Therapeutics and Innovation, Chongqing University of Arts and Sciences, Chongqing, 402160, China. E-mail: 18883138277@163.com

Bo Fang and Chunsheng Hu contributed equally to this work.

Abstract. In this study, we describe the discovery of the 4*H*-thieno[3,2-*b*]pyrrole derivatives as a useful scaffold to obtain potent lead compounds for the treatment of colon cancer. We first started with the 4*H*-thieno[3,2-*b*]pyrrole derivatives which come from compound libraries screening, and then optimized their structures based on the cellular activities and pharmacophore models. The inhibition rate of cell growth assay demonstrated that this series compounds showed better inhibitory activities against colon cancer cells than other tested tumor cells. Moreover, the target of the most active compound **8i** was explored by target fishing strategy and validated by molecular docking and biological activity analysis. The results of apoptosis and flow cytometry demonstrated that compound **8i** induce cell apoptosis probably by inhibiting activity of methionine aminopeptidase 2, therefore compound **8i** may be a potent inhibitor to methionine aminopeptidase 2.

Keywords: Thieno[3,2-*b*]pyrrole derivatives; Colon cancer; Structure optimization; Target prediction; Methionine aminopeptidase 2

1. Introduction

Colon cancer is the third most commonly diagnosed cancer globally, and ranks among the three most important causes of cancer-related mortality worldwide.[1] Current colon treatment options include surgery, radiation therapy, and chemotherapy. Due to the lack of an early diagnosis, most patients are not eligible for surgical resection.[2,3] In addition, a major drawback of the use of cancer chemotherapy results from the lack of tumor specificity shown by most anticancer drugs.[4] Therefore, new and effective anticancer drugs are required for the management of colon carcinoma.

As an effective means of discovering novel lead compounds, screening compound libraries for specific targets or cells is a powerful technique for identifying hit molecules as starting points in drug research and development.[5-8] Therefore, to address the increasingly severe situation of colorectal cancer, we try to find suitable lead compounds by using the method of compound library screening which will be introduced in detail below, and optimize the structure of lead compounds to obtain the potential compounds which deserve further research and development. The screening results suggest that the inhibition rates of compounds **I**-**IV** are more than 50% on typical colorectal cancer cells (HT29 and/or HCT116) (Figure 1), moreover, the shared feature of these compounds is 3-phenyl-4*H*-thieno[3,2-*b*]pyrrole skeleton.

Although some literatures reported that several 4*H*-thieno[3,2-*b*]pyrrole derivatives showed antitumor, antidiabetic and antiallergic effects by targeting LSD1,[9,10] CHK1,[11] CENP-E,[12] glycogen
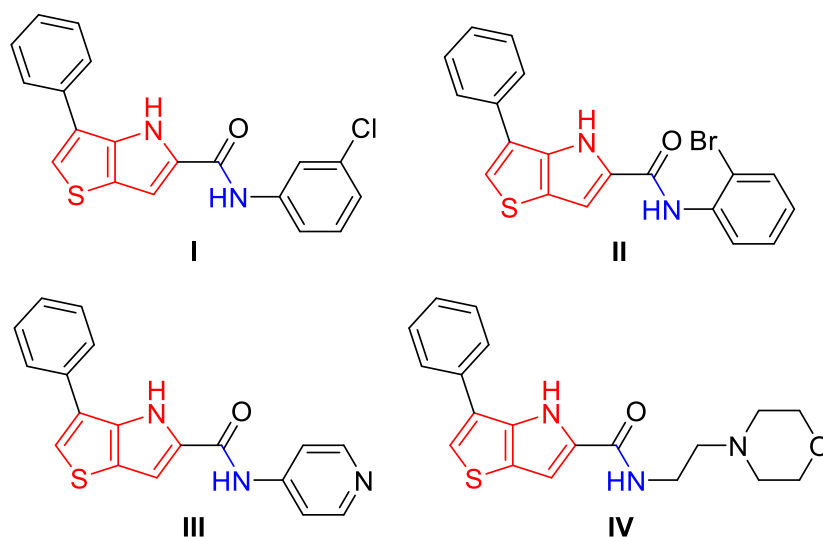
**Figure 1.** Four potent lead compounds from preliminary inhibition rates screening experiment.

Phosphorylase,[13,14] Human Histamine H4[15] etc., to date there is no clinic drugs containing 4*H*-thieno[3,2-*b*]pyrrole scaffold which fused by pyrrole and thiophene groups. Therefore, the 4*H*-thieno[3,2-*b*]pyrrole derivatives may have special pharmacological properties due to their chemical structure obvious difference from current drugs. Given the necessity of developing new anti-colon cancer drugs and the possible biological activities of 4*H*-thieno[3,2-*b*]pyrrole derivatives based on the results of the compound libraries screening, we designed and synthesized a series of 4*H*-thieno[3,2-*b*]pyrrole derivatives and studied their anti-tumor properties. Furthermore, in view of their potential in anti-colon cancer, we also explored the possible targets of these compounds through reverse targeting strategy and verified the result by molecular docking and biological experiments. These studies will provide valuable choices for molecular biologists and the pharmaceutical industry.

2. Results and Discussion

2.1. Discovery of Lead Compounds

It is generally known that computer-aided drug design (CADD) can find lead compounds through virtual screening at low cost with the fast pace of the development of computer technology in the field of drug research and development. However, due to the intricate mechanisms between drug molecules and biological cells, there is still a large gap between the measured and predicted activities of most of the lead compounds found by CADD. Therefore, it is still an effective way to find lead compounds with new structural characteristics by measuring the activities of compounds library molecules. Herein, we tested the inhibition rate of no less than 400 drug-like molecules on common tumor cells by screening typical commercial drug-like compounds library, the related tumor cells include Hela (cervical cancer cell),

Table 1. The inhibition rate of cell growth assay of first series of target conmounds (20μM) on common tumor cells[a].
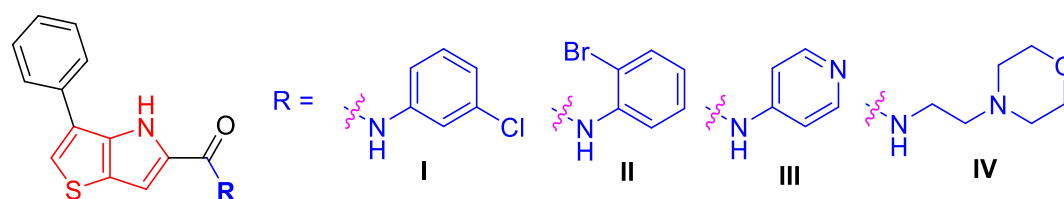
Compd.	Hela	U87	H1975	MCF-7	Hep3B	HT29	HCT116
I	23.89	25.09	60.08	54.25	35.05	70.22	72.27
II	0.62	62.30	13.04	56.38	16.75	14.15	52.63
III	57.89	59.39	44.85	62.97	46.18	66.78	69.25
IV	1.66	-0.76	14.78	2.37	7.88	65.58	2.90
Erlotinib	34.32	42.56	54.91	38.75	26.67	24.27	41.66
Paclitaxel	53.25	69.82	56.86	46.59	38.93	69.03	53.35

[a] The data were presented from three independent experiments.

U87 (glioma cell), H1975 (lung carcinoma cell), MCF-7 (breast cancer cell), Hep3B (hepatoma cell), HT29 and HCT116 (colon cancer cell). Since the target of this series of compounds is not yet clear, the typical small molecule targeted drug **Erlotinib** and natural broad-spectrum anticancer drug **Paclitaxel** were chosen as positive control drugs.

The results showed that most of compounds library molecules showed weak or no activity against these tumor cells. However, some compounds containing 4*H*-thieno[3,2-*b*]pyrrole skeleton (**I-IV**, Table 1) showed strong inhibitory activity on colon cancer cells. In particular, the inhibitory rates of compounds **I**, **III** and **IV** on HT29 at 20 μM were 70.22%, 66.78% and 65.58%, while the inhibitory rates of compounds **I**, **II** and **III** on HCT116 at 20 μM also reached 72.27%, 52.63% and 69.25%, respectively. These results showed that this kind of compounds has the potential to be lead compounds, especially compounds **I** and **III** showed strong inhibitory activities against both colon cancer cells, which were superior to or equivalent to the control drugs **Erlotinib** and **Paclitaxel**. Therefore, based on these compounds with 4*H*-thieno[3,2-*b*]pyrrole skeleton structure, we plan to carry out structural optimization on this kind of compounds in order to discover more active anti-tumor compounds and study their preliminarily mechanism of action.

2.2. Chemistry

The synthetic route of the target compounds **8a-8n** is outlined in Schemes 1. Methyl 2-chloroacetate **1** reacted with sodium azide in acetone and water at 60 °C to give methyl 2-azidoacetate **2** in yield of 85%, the following condensation of compound **2** and 4-bromothiophene-2-carbaldehyde **3** at the present of sodium methanolate in mehanol to produce methyl-2-azido-3-(4-bromothiophen-2-yl)acrylate **4** in yield of 65%, then methyl 3-bromo-4*H*-thieno[3,2-*b*]pyrrole-5-carboxylate **5** was obtained in yield of 82% by intramolecular cyclization of compound **4** in xylene under reflux. After this, compound **5** reacted with phenyboronic under conventional coupling reaction condition to give methyl 3-phenyl-4*H*-thieno[3,2-*b*]pyrrole-5-carboxylate **6** in yield of 60%, then hydrolyzed by sodium hydroxide aqueous solution and acidized by hydrochloric acid to give the key intermediate 3-phenyl-4*H*-thieno[3,2-*b*]pyrrole-5-carboxylic acid **7** in yield of 96%. Finally, target compounds **8a-8n** were prepared in yields ranging from 52% to 88% by condensation reaction of compound **7** with various amine at the present of dimethylaminopyridine, 3-(3-dimethylaminopropyl)-1-ethylcarbodiimide hydrochloride and 1-hydroxy-benzotriazole in dimethyl formamide.

As shown in scheme 1, we first synthesized four compounds for the preliminary biological activities
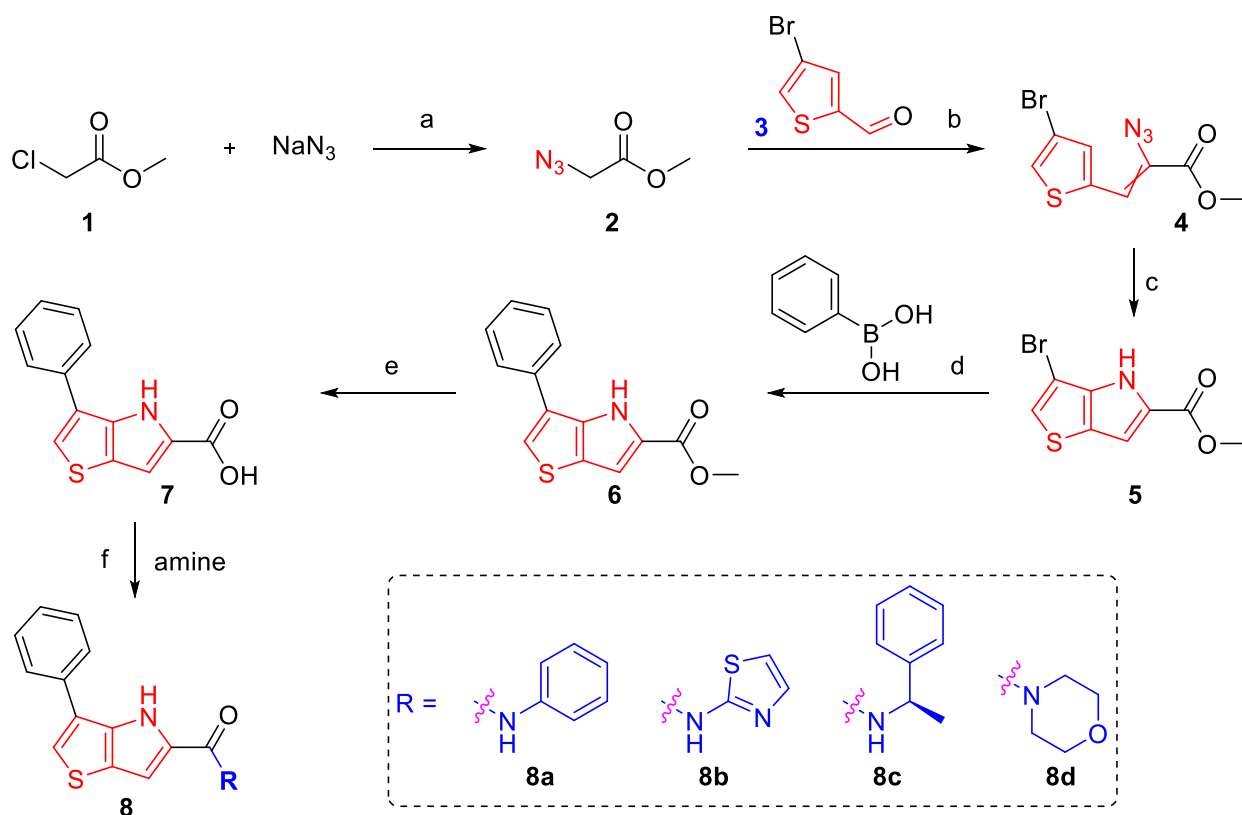
Scheme 1. Reagents and conditions: (a) acetone, H$_2$O; (b) NaOMe, MeOH; (c) xylene, reflux; (d) Pd(PPh$_3$)$_4$, Na$_2$CO$_3$, toulene, EtOH, H$_2$O, 100 °C; (e) NaOH, H$_2$O, then HCl; (f) Opportune amine, DMAP, EDCI, HOBT, DMF.

evaluation, which was used to compare with compounds **I-IV** and optimize the structure of the target molecules. The amines which were chosen for coupling with intermediate **7** are based on the following considerations (together with compounds **I-IV**): (a) To investigate the influence of various amines to the biological activities, the species of amines including aromatic amines, benzylamines and aliphatic amines; (b) To explore the effect of the aryl groups in aromatic amines and benzylamines, the aryl group could be (halogenated)phenyl, pyridyl, thiazolyl and so on. Therefore, based on the structures of compounds **I-IV**, four amines were used to synthesize the target compounds, and all these compounds were investigated the cell viabilities to typical tumor cells by MTT assay.

The cell viability data was shown in Table 2, these results not only showed that these compounds may exhibit more potential in against colon cancer cells (HT29 and HCT116) than other tumor cells, but also revealed that the biological activities of these compounds was strongly associated with the kinds of their amino groups, and more specifically, aromatic amine groups of target compounds (**I** and **III**) are superior moieties than corresponding benzylamine and alkyl amine groups (**IV**, **8c** and **8d**) based on these biological data. In additon, the different aryl in aromatic amine groups make the compounds exhibiting different biological activities, for instance, six-membered aromatic ring such as (halogenated)phenyl and pyridyl (**I-IV** and **8a**) are more beneficial to improve the biological activities of target compounds than five-membered aromatic ring (**8b**). Moreover, the inhibitory activities of compound **8a** on cells HT29 and HCT116 were significantly better than the control drug **Erlotinib**, and were comparable to the control drug **Paclitaxel**.

Table 2. The inhibition rate of cell growth assay of first series of target conmounds (20μM) on common tumor cells[a].
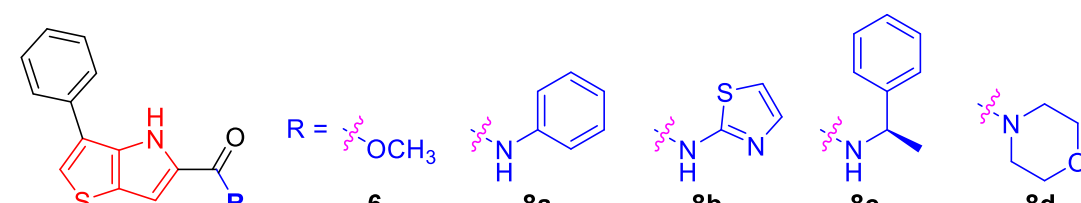
Compd.	Hela	U87	H1975	MCF-7	Hep3B	HT29	HCT116
6	44.64	40.53	9.32	-1.81	1.32	47.64	37.43
8a	17.00	36.66	38.12	39.39	8.04	63.53	59.03
8b	8.44	0.40	31.03	28.70	2.14	32.29	15.02
8c	3.40	38.72	16.25	21.49	1.38	59.19	39.13
8d	2.04	4.68	5.62	8.30	-0.96	7.24	10.84
Erlotinib	34.32	42.56	54.91	38.75	26.67	24.27	41.66
Paclitaxel	53.25	69.82	56.86	46.59	38.93	69.03	53.35

[a] The data were presented from three independent experiments.
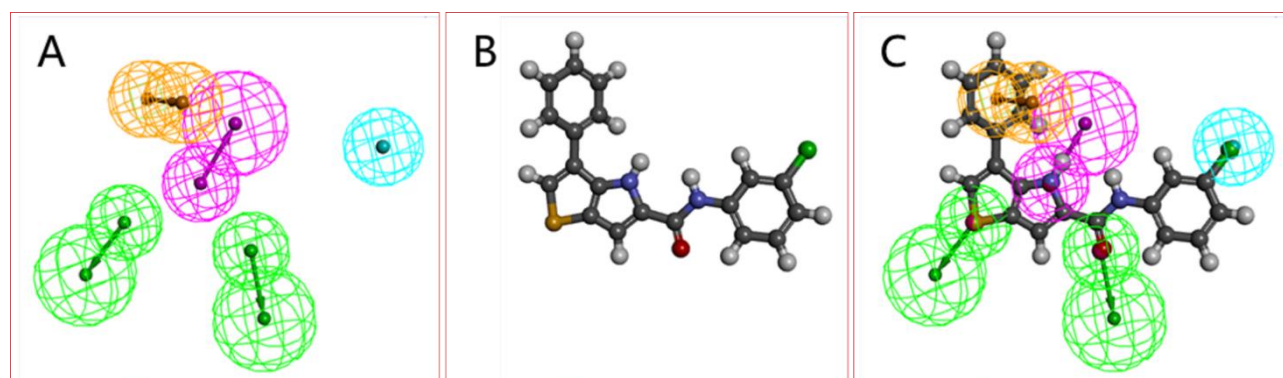
Figure 2. HipHop pharmacophore model for training set. (A) The best HipHop pharmacophore model. (B) The configuration of the most active compound **I**. (C) The best HipHop model mapped with the most active compound **I** in the training set. The features are color coded with green (hb_acceptor); magenta (hb_donor); yellow (ring_aromatic feature); light blue (hydrophobic feature).

Furthermore, it's well known that pharmacophore model is widely applied to explore common chemical characteristics among a considerable number of structures with great diversity and used as a query for searching chemical databases and finding new chemical entities.[16,17] Therefore, the pharmacophore model of these compounds was generated based on their cytotoxic activities in order to better understand corresponding structure-activity relationships and effectively optimize the structure of target compounds furtherly using the HipHop module from Discovery Studio 2018 package. The Feature Mapping tool was used firstly to generate all pharmacophore feature of these compounds, the 'principal' and 'MaxOmit-Feat' values were 2 and 0 for high active compounds (**I** and **III**), 1and 1 for moderate activite compounds (**8a**), 0 and 2 for low active compounds (**6**, **II**, **IV** and **8b-8d**) respectively, these compounds form the training set. The pharmacophore feature includes acceptor (HBA), donor (HBD), hydrophobe (H), ionizable positive and ring aromatic which will be used for generating HipHop pharmacophore model by Common feature Pharmacophore generation. The parameter settings are as follows: conformation generation (best), maximum conformations (200), energy threshold (10), features (hb_acceptor, hb_donor, hydrophobic, pos_ionizable and ring aromatic), and the rest HipHop parameters were kept at their default values. The top ten hypotheses were generated based on the training set molecules using Common Feature Pharmacophore Generation to identify the common features necessary to responsible for a desired biological activity. Figure 2A shows the best HipHop pharmacophore hypothesis, which contains five features: two hydrogen-bond acceptors, one hydrogen-bond donor, one aromatic moiety and one hydrophobic feature, and figure 2B displays the steric configuration of the most active compound **I**. In addition, figure 2C presents the mapping of the pharmacophore model onto the most active compound **I** in the training set. The HipHop pharmacophore hypothesis explicitly demonstrated the importance of hb_donor, hb_acceptor, ring_aromatic moiety and hydrophobic feature. Therefore, more kinds of amines will be used to synthesize the following target compounds for investigating their effect on biological activities, these newly synthesized compounds will be served as a test set to validate the reliability of the HipHop pharmacophore model.

Table 3. The inhibition rate of cell growth assay of second series of target conmounds (20μM) on common tumor cells[a].
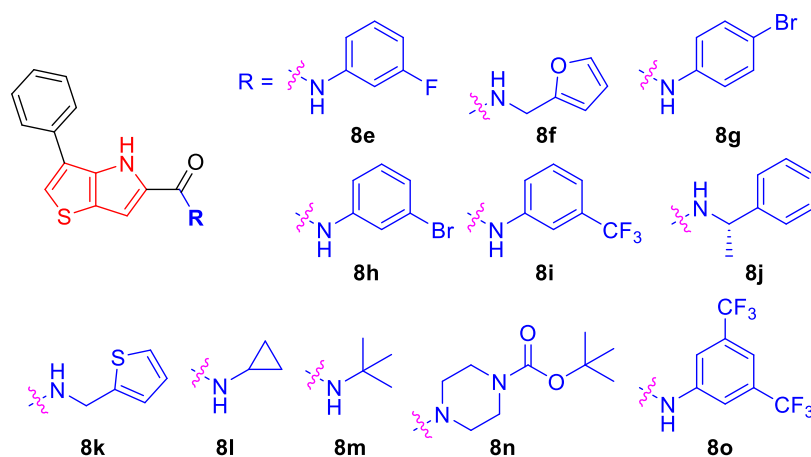

| Compd.	Hela	U87	H1975	MCF-7	Hep3B	HT29	HCT116
8e	26.58	32.54	51.60	52.95	26.89	68.95	78.52
8f	6.87	30.52	6.09	8.20	11.24	69.07	32.69
8g	32.69	31.79	57.58	54.31	31.98	67.69	72.20
8h	32.33	21.91	56.16	55.87	33.28	74.42	73.86
8i	67.46	48.28	78.87	66.97	70.44	76.23	86.41
8j	1.20	42.03	2.21	4.55	1.49	50.30	5.18
8k	-2.86	3.45	12.75	21.93	10.53	66.17	34.83
8l	1.70	1.73	12.29	3.55	2.31	39.39	8.64
8m	43.83	22.55	22.15	31.18	12.69	34.74	7.03
8n	6.18	1.25	8.19	1.08	3.58	5.85	19.41
8o	19.56	43.47	65.43	35.91	15.52	75.97	58.64
Erlotinib	34.32	42.56	54.91	38.75	26.67	24.27	41.66
Paclitaxel	53.25	69.82	56.86	46.59	38.93	69.03	53.35

a) The data were presented from three independent experiments.

Due to hydrophobic feature of compounds plays a very important role in HipHop pharmacophore model, introducing more hydrophobic groups such as various halogen and alkyl groups into target compounds may be an effective strategy to improve their potency for tumor inhibition. Therefore, based on above HipHop pharmacophore model, ten target compounds were synthesized and their biological activities have been evaluated, the data of cell viability assay was shown in table 3, the result demonstrated that this series compounds also showed better inhibitory activities against colon cancer cells than other tumor cells. The inhibitory activities of compounds **8e**, **8g-8i** against colon cancer cells suggested that these compounds may be potential lead compounds in the study of new drugs against colon cancer. Especially, compound **8i** is a most active compound against colon cancer cells and almost have high inhibitory activities to all tested tumor cells, not only that, the inhibitory activities of compound **8i** on all tested tumor cells have completely surpassed control drugs **Erlotinib** and **Paclitaxel** except the inhibitory activity of compound **8i** on cell U87 is slightly lower than control drug **Paclitaxel**. Therefore, compound **8i** was chosen for further studying to reveal its anti-tumor mechanism.
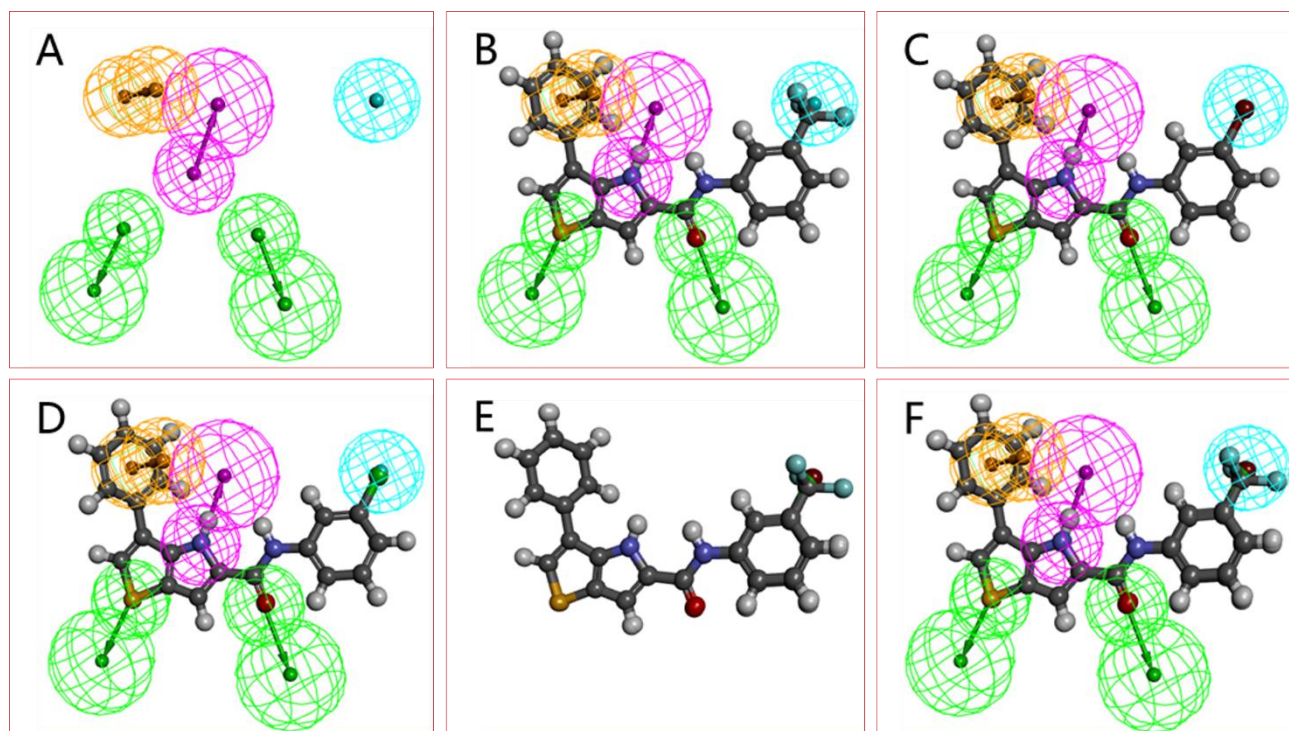
Figure 3. HipHop pharmacophore model for test set. (A) The best HipHop pharmacophore model Hypo10. (B) The Hypo10 mapped with the most active compound **8i**. (C) The Hypo10 mapped with compound **8h**. (D) The Hypo10 mapped with compound **I**. (E) The overlapped conformation of three most active compounds (**8i**, **8h** and **I**). (F) The Hypo10 mapped with three active compounds (**8i**, **8h** and **I**). The features are color coded with green (hb_acceptor); magenta (hb_donor); yellow (ring_aromatic feature); light blue (hydrophobic feature).
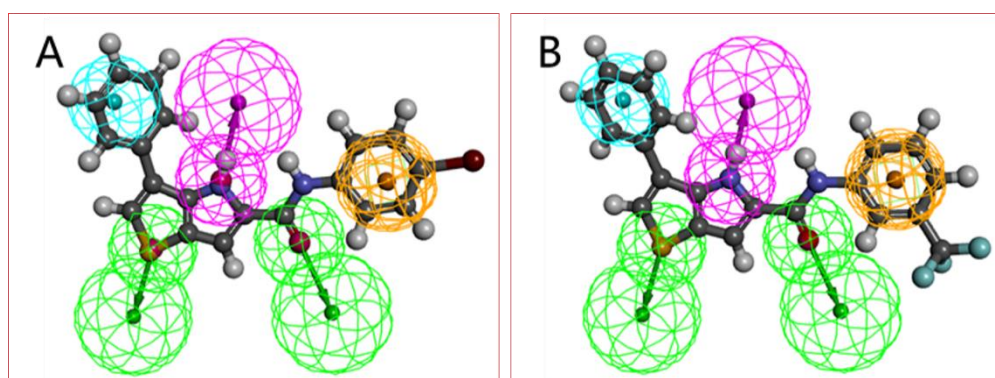
Figure 4. (A) Compound **8g** of the test set mapped to Hypo3. (B) The most active compound **8i** of the test set mapped to Hypo3. The features are color coded with green (hb_acceptor); magenta (hb_donor); yellow (ring_aromatic feature); light blue (hydrophobic feature).

Because the structural optimization strategy for the second series of compounds is based on the HipHop pharmacophore model established by the first series of compounds (training set), so the second series of compounds will be serve as the test set to validate the reliability of HipHop model by using Ligand Profiler tool, the parameter settings are as follows: input file pharmacophores (above ten pharmacophores), conformation generation (best), maximum conformations (200), energy threshold (10), save conformations (true), maximum omitted features (-1), scale fit values (false), aligned ligands (true) and the rest parameters were kept at their default values. Surprisingly, the results of Ligand Profiler are in good agreement with the experimental values, that is to say, most of the active compounds can match the model very well, these properties can also be seen from Figure 3 which depicted the conformations of compounds **8i**, **8h** and **I** mapped onto Hypo10. Especially, compound **8i**, as the most active compound, successfully fit all chemical features in the Hypo10 model, and is the most matched compound in all ten models. Additionally, the trifluoromethyl of compound **8i**, as the hydrophobic group, have significant effect to improve the inhibitory activities, we can also see that one hydrophobic feature was overlapped with the trifluoromethyl moiety. However, we must recognize that just relying on single pharmacophore model (Hypo10) may not match all compounds perfectly, such as highly active compound **8g** couldn't match well with pharmacophore of Hypo10. Even so, there

is one other pharmacophore model (Hypo3) in HipHop may explain why compound **8g** exhibits high activities. As shown in Figure 4, compound **8g** fit all features of Hypo3 very well, in particular, the aromatic feature may be overlapped by 4-bromophenyl ring very well. Additionally, the most active compound **8i** was still the best matched compound in Hypo3. These evidences illustrated that the strategy of optimizing the structure of compounds through the HipHop pharmacophore model was feasible.

In order to study the possible target of this kind of compounds, the most active compound **8i** was used as ligand to search the potential target by reverse virtual screening, also known as *in silico* or computational target fishing.[18] Furthermore, the result of the reverse virtual screening will be verified by molecular docking.

Table 4. The pharmacophores and corresponding fitvalues of the target prediction screening[a].

Compound	Pharmacophore	Fitvalue
8i	1KQ0-01	4.45067
	3D15-03	4.42972
	3D7Z-03	4.40169
	3D2K-02	4.26285
	3DKO-06	4.26164
	1WBT-05	4.21522
	3DJ7-03	4.18110

[a] The best five pharmacophores were presented.
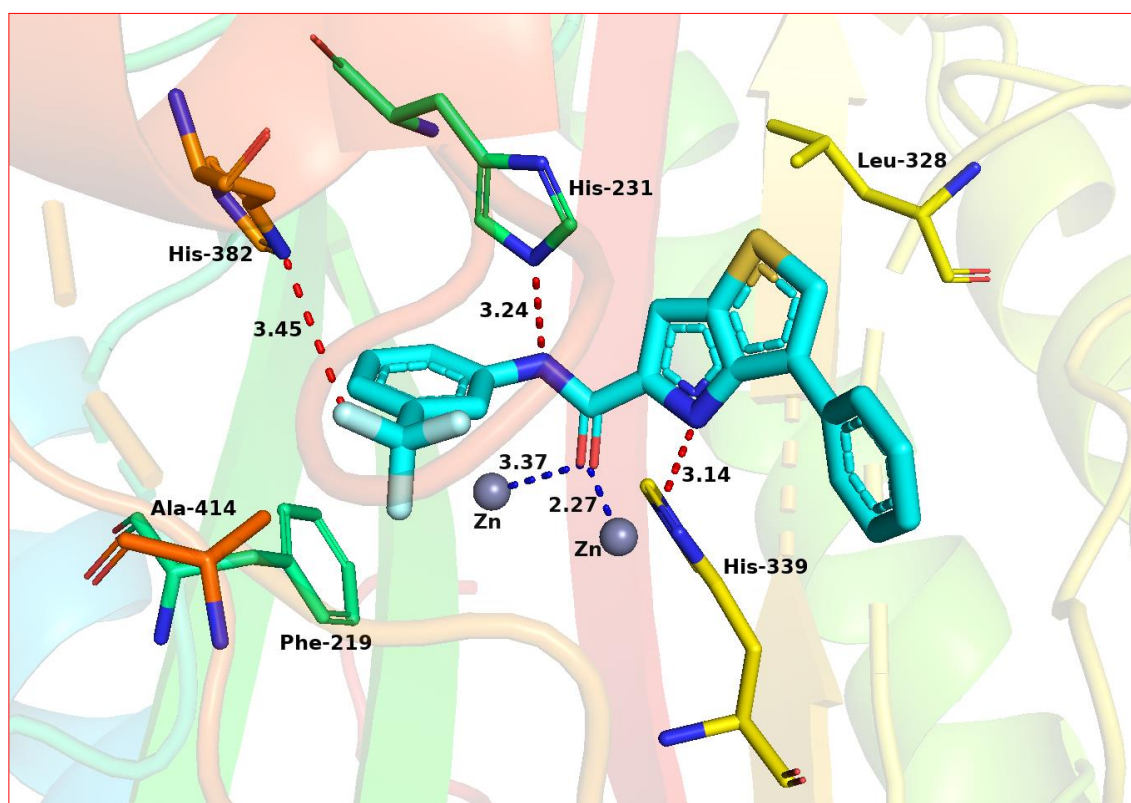
Figure 5. 3D conformations of compound **8i** docked into methionine aminopeptidase 2 (PDB code: 1KQ0).

Herein, the Ligand Profiler module, which was based on the reverse pharmacophore searching method, will be used to predict the potential target of compound **8i** by reverse virtual screening. The parameter settings are as follows: Input Ligands (compound **8i**), Input PharmaDB Pharmacophores (All (noshape and shape)), Model Selection (All Models), Conformation Generation (FAST), Maximum Omitted features (-1), Save Aligned Ligands (true) and the rest parameters were kept at their default values. The calculation result (Table 4) indicated that there are two pharmacophore models (1kq0-1 and 3d15-3) related to cancer with the highest Fitvalues, which indicated that methionine aminopeptidase 2 (METAP2) or auroral kinase A might be the target of compound **8i**. The results of biological experiments suggested to us that compound **8i** could exert inhibitory effects on tumor cells probably relating to cell apoptosis but not cell cycle. Therefore, METAP2 will be used in molecular docking to study its possible mechanisms of action.

The CDOCKER module in DS2018 was utilized to perform the probable interaction between compound **8i** and methionine aminopeptidase 2. A high resolution crystal structure of METAP2 bound with an inhibitory molecule, A849519 (PDB code 1KQ0) was selected for molecular docking studies. All water molecules were removed from 1KQ0 before docking calculations. In the protein structure hydrogen atoms were added and CHARMm forcefield was applied for energy minimization. Binding site present in the protein was defined within the radius of 7.0 Å. For convenience of comparison, two most active compounds (**8i** and **8h**) were docked into the crystal structure of METAP2 enzyme and top ten poses were examined on the basis of CDOCKER INTERACTION ENERGY (protein–ligand interaction energy) to evaluate the nature and type of interactions. It was observed that compound **8i** docked very well with a CDOCKER INTERACTION ENERGY of -51.57. As shown in Figure 5 and 6, we may see that there were two NH groups and one fluorine atom in compound **8i** showed three hydrogen bonds interaction with His339, His231 and His382 with the distance of 3.14 Å, 3.24 Å and 3.45 Å respectively. Additionally, the oxygen atom of carbonyl group in compound **8i** showed metal-acceptor interaction with two zinc ion. Six amino acids namely Ala414, Phe219, His339, His231, His382 and Leu328 made the hydrophobic environment around compound **8i** (Figure 6). Furthermore, compound **8h** also showed prominent interaction (Figure 7) with a good CDOCKER INTERACTION of -36.76. Similar to compound **8i**, there were two hydrogen bonds (2.94 Å to His-339 and 3.51 Å to Asp-262), two metal-acceptors interaction (2.17 Å and 2.10 Å) and hydrophobic environment between compound **8h** with METAP2. However, compound **8i** showed better docking capacity with METAP2 than compound **8h** based on the data of CDOCKER INTERACTION ENERGY and hydrogen bond. These results theoretically explain why compound **8i** has better inhibitory activities in colon cancer cells than compound **8h**, and have been confirmed in further biological experiments.
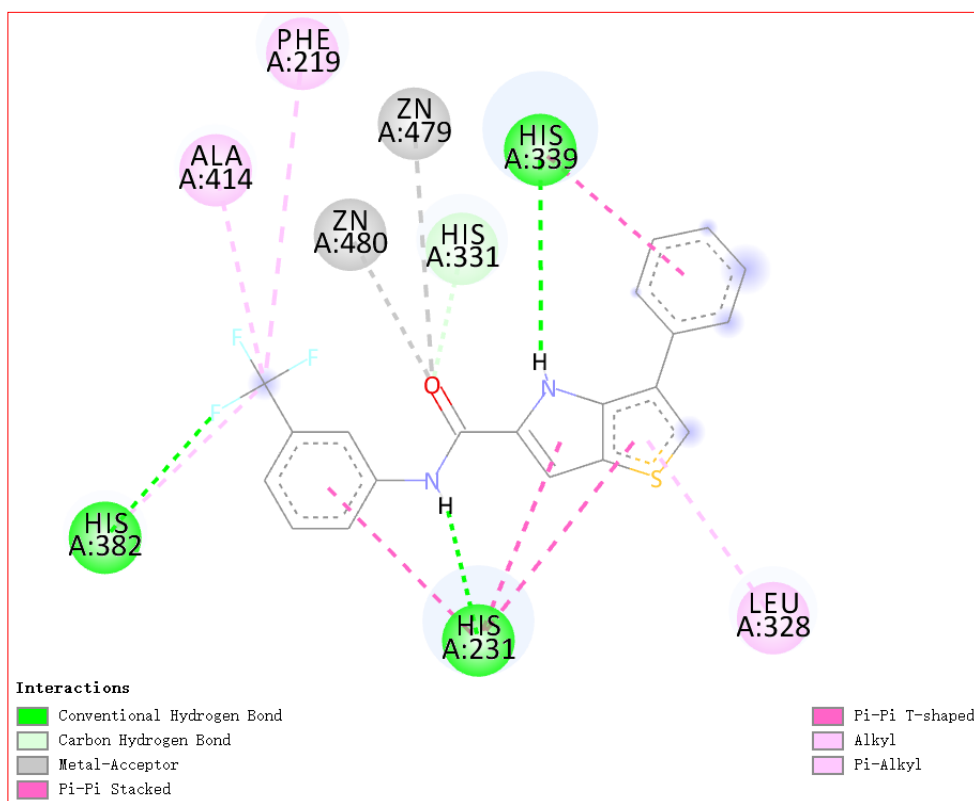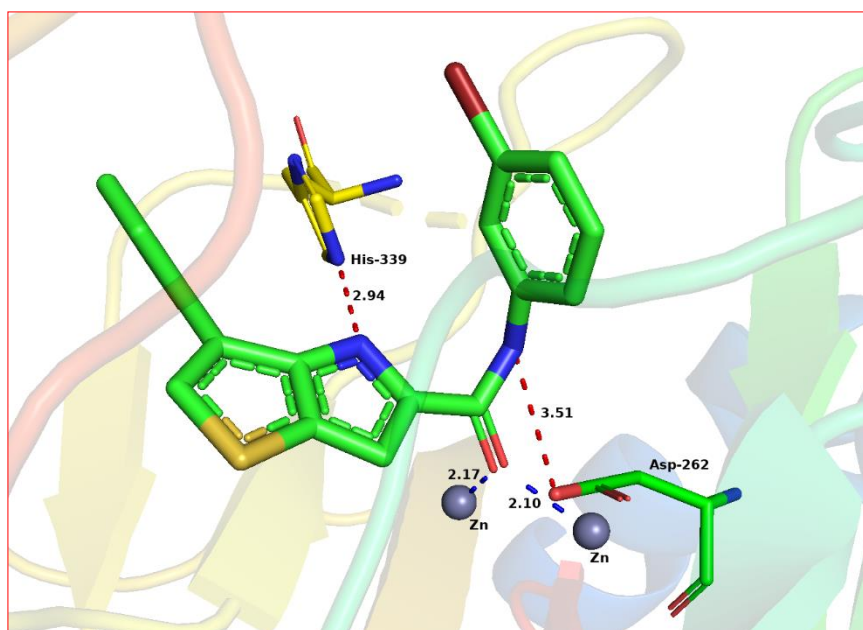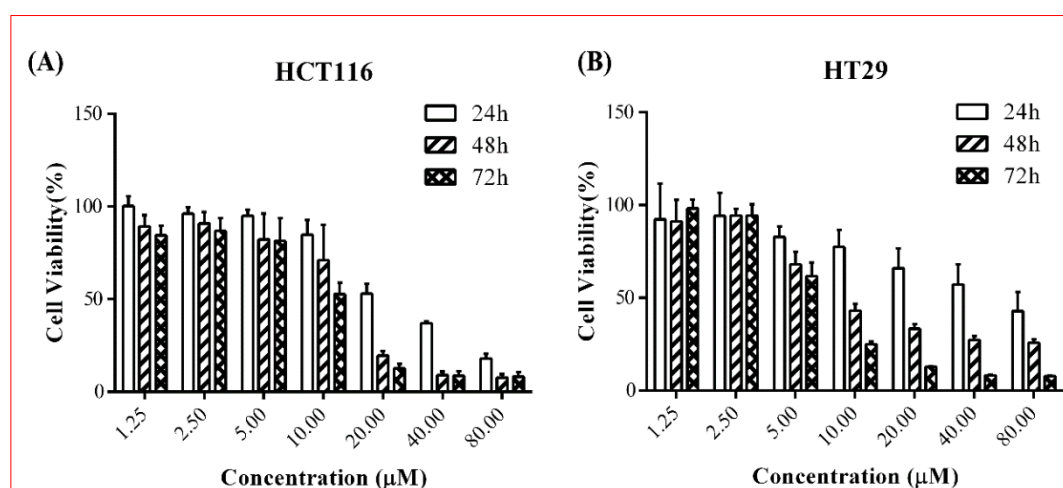

Figure 6. 2D conformations of compound **8i** docked into methionine aminopeptidase 2 (PDB code: 1KQ0).

Figure 7. 3D conformations of compound **8h** docked into methionine aminopeptidase 2 (PDB code: 1KQ0).


Figure 8. Cytotoxic activities of compound **8i** against human colon cancer HCT116 and HT29 cells. Dose- and time- dependent anti-proliferative activities of compound **8i** against HCT116 and HT29 cells. The values represent the means of three separate experiments.

The anti-proliferative effect of compound **8i** on the viability of HCT116 and HT29 cells were assessed using the MTT method. As shown in Figure 8, we treated compound **8i** at different times and doses and it inhibited the growth of HCT116 and HT29 cells in a time- and dose-dependent manner. As a result, compound **8i** was found to have anticancer activities after 48h treatment in HCT116 and HT29 cells at an IC$_{50}$ of 10.93 and 6.25μM, respectively. However, compound **8i** did not show obvious cytotoxicity at 100μM against normal colon FHC cell. Next, the role of compound **8i** in the regulation of colony formation ability of HCT116 and HT29 cells were investigated. As shown in Figure 9, compound **8i** significantly inhibited the colony formation of HCC116 and HT29

cells in dose-dependent manner.

Compound **8i** was docked into human MetAP2 according to the result of target prediction and molecular docking. Previously researches reported that MetAP2 has been found to be overexpressed in colon cancer cell lines and in samples from colon cancer patients when compared to normal tissue.[19-21] Moreover, various reports suggested that MetAP2 plays a critical role in cell proliferation and tumor growth. Downregulation of MetAP-2 expression significantly induces apoptosis in rat hepatoma cells.[22] To determine whether the growth inhibitory effect of compound **8i** is associated with the induction of apoptotic cell death by inhibition of MetAP2 activity, flow cytometry was
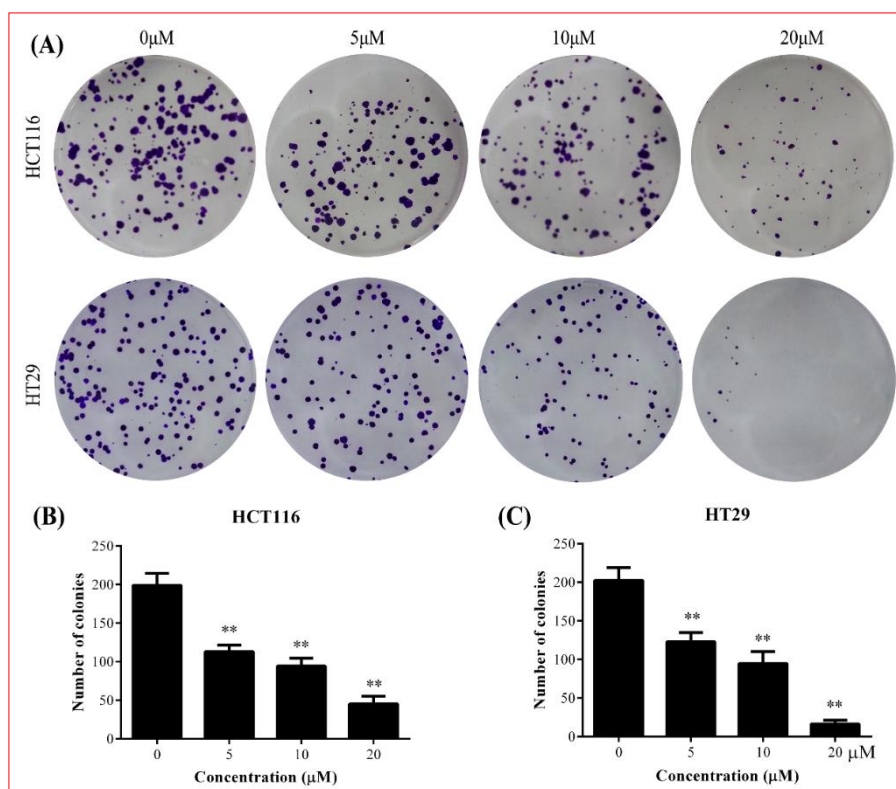
Figure 9. Compound **8i** inhibited HCT116 and HT29 cancer cells colony formation. (A) The image of HCT116 and HT29 cancer cells colony formation with compound **8i** at concentration of 0, 5, 10 and 20 µM. (B and C) The number of colonies was counted in per plate. data presented are representative of those obtained in at least three separated experiments. **P＜ 0.01 vs group with 0 µM compound **8i**.

performed. HCT116 and HT29 cells were exposed to various concentrations (0, 5, 10 and 20 µM) of compound **8i** for 48 h and analyzed using propidium iodide (PI)/Annexin V double staining followed by flow cytometry.

As shown in Figure 10, we observed a dose-dependent increase in apoptotic cells in the presence of compound **8i** in HCT116 and HT29 cells. The results showed that the HCT116 cell was more sensitive to compound **8i** than HT29. The apoptotic cell death of HCT116 was upto 32.96%, 30.52% and 67.64% after incubation with compound **8i** at 5, 10 and 20 µM, respectively. The apoptotic cell death of HT29 was upto 13.03%, 15.82% and 26.89% after incubation with compound **8i** at 5, 10 and 20 µM, respectively. As a result, these data indicated that the primary mode of cell death is through apoptosis, which is induced by inhibition of MetAP2 activity with the compound **8i**.

The mitochondrial or intrinsic apoptosis pathway was mediated by pro-apoptotic proteins (such as Bax and PARP) and anti-apoptotic proteins (such as Bcl-2 and p-Bad). MetAP2 also affects the pathway of apoptosis by regulation of Bcl-2 protein expression.[23] Inhibition of MetAP2 in mesothelioma cells depresses both mRNA and protein expression of the Bcl-2.[21] Previously studies suggested that MetAP2 plays a major role in proliferative and apoptosis pathways.[21,24,25]

As shown in Figure 11, the levels of pro-apoptotic proteins Bax and PARP were markedly increased in HCT116 and HT29 cells by compound **8i** treatment, whereas levels of anti-apoptotic proteins Bcl-2 and p-Bad were reduced compared with the DMSO control. The Bax/Bcl-2 ratio is an important factor for regulating mitochondrial cytochrome C release and is usually used as an indicator of cells apoptosis. The dysregulation of the balance between proliferation and cell death represents a pro-tumorigenic principle in human colon cancer.[26] Apoptosis plays an important role in regulating the development, homeostasis, and elimination of unwanted and malignant cells. It is a valuable therapeutic method in clinical practice that inducing apoptosis in human colon cancer cells via inhibition of the anti-apoptotic factor, Bcl-2, or the activation of a pro-apoptotic factor, Bax, which induces activation of mitochondrial apoptotic pathways.[27-29] In addition, Bax is localized in the cytoplasm and mitochondrial membrane, inducing release cytochrome C into the cytosol followed by recruitment and activation of caspases to lead to cell apoptosis.[30,31] Our results consistent with the previous reports indicated that Bax/Bcl-2 ratio was increased by compound **8i** treatment, which regulated HCT116 and HT29 cells apoptosis by mitochondrial cytochrome C pathway.
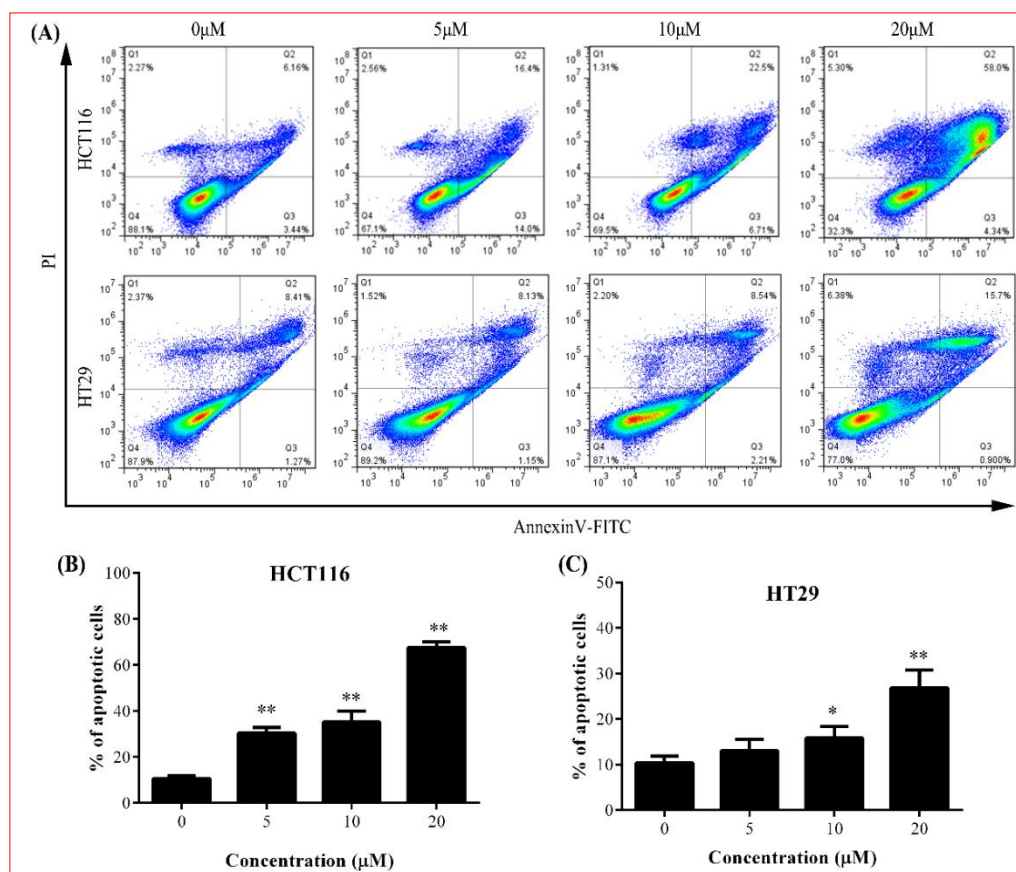
Figure 10. Apoptosis driven effects of compound **8i** against HCT116 and HT29 cells. (A) HCT116 and HT29 cells were collected for flow cytometry analysis after incubated with compound **8i** at different concentration for 48h. (B and C) The graph showed cell apoptosis rates at 0, 5, 10 and 20 μM compound compound **8i**. *P＜0.05, **P＜0.01 vs group with 0μM compound **8i**.
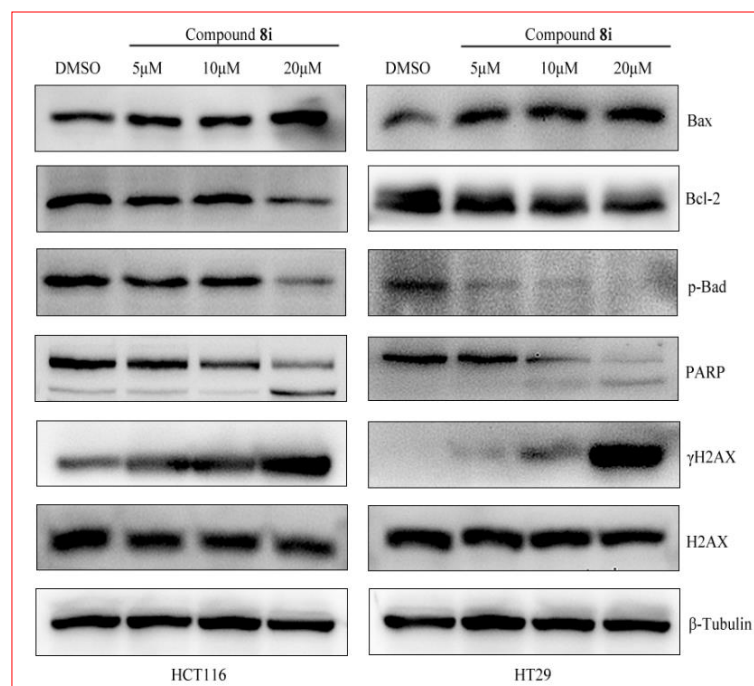
Figure 11. Effects of compound **8i** on protein expression in HCT116 and HT29 cells. Cancer cells were incubated with compound **8i** at concentration of 0, 5, 10 and 20 μM for 48 h. β-tubulin was used for normalization. Western blot data presented are representative of those obtained in at least three separated experiments.
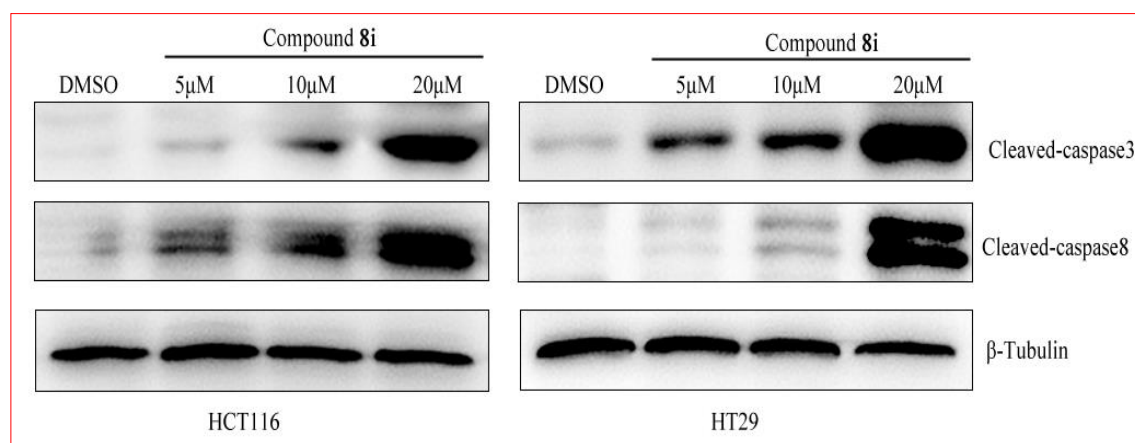
Figure 12. compound **8i** induced caspase3 and 8 activation in HCT116 and HT29 cells. Cancer cells were incubated with compound **8i** at concentration of 0, 5, 10 and 20 μM for 48 h. β-Tubulin was used for normalization. Western blot data presented are representative of those obtained in at least three separated experiments.

Phosphorylation of H2AX, called γH2AX, is recognized as an excellent marker of DNA DSBs.[32] γH2AX was reported to be a useful tool to monitor the response of patients to cancer therapy by genotoxic chemicals. Because γH2AX is also generated by apoptosis, a γH2AX-assay might assess genotoxic risk incorrectly [33]. Therefore, we investigated capacity of compound **8i** to induce apoptosis on measurements of γH2AX by western blot. The data showed that the expression of γH2AX was increased with dose-dependent increase of compound **8i** (Figure 11).

The MetAP2 is overexpression in Colon adenocarcinoma HCT116 and HT29 cell lines, which is responsible for the reported reduction in protein levels of caspase cascades.[21,24] A hand of studies reported that caspase cascades are crucial effectors and mediators of apoptosis induction and caspase3 and 8 have been linked to mitochondrial death pathway,[34-36] therefore the expression of cleaved-caspase3 and 8 in HCT116 and HT29 cells were analyzed. The data revealed that treatment with compound **8i** increased the activities of caspase3 and 8 in both colon cancer cell lines to a significantly greater extent than untreated cells (Figure 12). Apoptosis disorders are an additional cause for the occurrence of colon cancer. The initiation of apoptosis is typically triggered via caspase3, which is being used to treat cancer. Therefore, compound **8i** which increase caspase3 and 8 activities or γH2AX expression by inhibition of MetAP2 activity, may be effective tools to improve colon cancer prognosis.

3. Conclusion

In summary, this paper presents researches of the discovery of 4*H*-thieno[3,2-*b*]pyrrole scaffold, the optimization of structure, the exploration of structure-activity relationship and the mechanism of action of the 4*H*-thieno[3,2-*b*]pyrrole derivatives based on the compound libraries screening, molecular docking and target fishing strategies. The results showed that compound **8i**, which bearing a hydrophobic trifluoromethyl group, was the most active compound against all tested tumor cell lines, especially in HCT116 (IC_{50} 10.93 μM) and HT29 (IC_{50} 6.25 μM) cells. The molecular biological target of compound **8i** was explored by target fishing strategy, the result demonstrated that methionine aminopeptidase 2 probably be the target of compound **8i**, which was further validated by molecular docking. The biological results suggested that compound **8i** induced the apoptosis of HCT116 and HT29 colon cancer cells probably through methionine aminopeptidase 2, and in accordance with the result of target fishing and molecular docking. This study provides valuable information for the development of new anti-cancer drugs and offer more options for biologists and pharmaceutical industries.

4. Experimental Section

4.1. Chemistry
^{1}H and ^{13}C NMR were recorded on a Bruker 400 spectrometer. The high-resolution mass spectra (HRMS) were recorded on an Thermo UItiMate 3000-Q Exactive mass spectrometer with ESI resource. LC-MS analyses were performed on a Shimadzu-2020 LC-MS instrument using the following conditions: Shim-pack VPODS C18 column (reverse phase, 150 x 2.0mm); 80% acetonitrile and 20% water over 6.0 min; flow rate of 0.4 mL/min; UV photodiode array detection from 200 to 300nm. The products were purified by Biotage Isolera™ Spektra Systems and *n*-Hexane/EtOAc or Dichloromethane/Methanol solvent systems. Microwave irradiation experiments were carried out in a Biotage® Initiator Classic microwave apparatus with continuous irradiation power from 0 to 400W with utilization of the standard absorbance level of 250W maximum power. The reactions were carried out in 5 or 10 mL glass tubes, sealed with microwave cavity. The reaction was irradiated at a required ceiling temperature using maximum power for the stipulated time. Then it was cooled to 50°C with gas jet

cooling. All reagents and solvents were obtained from commercial sources and used without further purification.

4.2. Synthesis

Methyl 2-azidoacetate (2)
To a solution of methyl 2-chloroacetate (1.09 g, 10.0 mmol) in acetone/water (20 mL, 2/1, v/v) was added NaN_3 (1.30 g, 20.0 mmol) at room temperature, after addition the mixture was heated to 60 °C for 3 hours, then the mixture was evaporated and the residue was extracted by ethyl acetate and wash by saturated $NaHCO_3$ solution and brine, dried and concentrated to give crude compound **2** as a light yellow oil (0.98 g, yield: 85%), which was used for next step without further purification.

Methyl (E)-2-azido-3-(4-bromothiophen-2-yl)acrylate (4)
To a solution of NaOMe (1.35 g, 25.0 mmol) in MeOH (10 mL) was added a solution of 4-bromothiophene-2-carbaldehyde (**3**, 1.91 g, 10.0 mmol,) and methyl 2-azidoacetate (2.42 mL, 25.0 mmol) in MeOH (10 mL) dropwise at -10 °C over 30 minutes and stirred for 2 hours at this temperature The mixture was allowed to stir for an additional 2.5 h at 0° C and then poured into ice-water, extracted with ethyl acetate, washed with water. The organic layer was dried over Na_2SO_4 and concentrated under reduced pressure. The residue was purified by column chromatography using ethylacetate/hexane (1:19) to yield pure product **4** (1.87 g, 65%).

Methyl 3-bromo-4H-thieno[3,2-b]pyrrole-5-carboxylate (5)
A solution of compound **4** (2.88 g, 10 mmol) in dry toluene (100 mL) was slowly added into boiling xylene (100 mL) over 1 h, then the reaction mixture was refluxed for an additional 3 h. After the reaction completed the mixture was cooled and the solvent was removed under reduced pressure. The residue was purified by column chromatography using ethylacetate/hexane (1:4) to yield pure compound **5** (2.13 g, 82%) .^{1}H NMR (400 MHz, DMSO-d6) δ 12.53 (s, 1H), 7.63 (s, 1H), 7.19 (s, 1H), 3.83 (s, 3H). ^{13}C NMR (101 MHz, DMSO) δ 161.41, 140.25, 127.95, 126.89, 123.47, 108.78, 94.55, 52.00. HRMS (E) calcd for $C_8H_7BrNO_2S^+$ [M+H]$^+$, 259.93754; found, 259.93787.

Methyl 3-phenyl-4H-thieno[3,2-b]pyrrole-5-carboxylate (6)
A mixture of compound **5** (2.08 g, 8.0 mmol), phenylboronic acid (1.22 g, 10.0 mmol), Na_2CO_3 (1.06 g, 10.0 mmol) and Pd(PPh$_3$)$_4$ (925 mg, 0.8 mmol) in toulene/EtOH (20 mL, 3/1, v/v) was degassed and protected by N_2, then the mixture was stirred at 100 °C for 40 minutes in microwave apparatus. After the reaction completed the mixture was dried and purified by column chromatography (ethylacetate/hexane = 1/5) to give compound **6** (1.23 g, 60%) as a yellow solid. ^{1}H NMR (400 MHz, DMSO-d_6) δ 12.15 (s, 1H), 7.79 (d, 7.7 Hz, 2H), 7.74 (s, 1H), 7.45 (t, J = 7.2 Hz, 2H), 7.37 (d, J = 6.8 Hz, 1H), 7.22 (s, 1H), 3.83 (s, 3H). ^{13}C NMR (100 MHz, DMSO-d_6) δ 161.56, 139.95, 133.79, 129.13, 127.85, 127.79, 127.57, 127.36, 126.05, 125.08, 108.62, 51.88. HRMS (E) calcd for $C_{14}H_{12}NO_2S^+$ [M+H]$^+$, 258.05833; found, 258.05856.

3-Phenyl-4H-thieno[3,2-b]pyrrole-5-carboxylic acid (7)
To a solution of compound **6** (1.54 g, 6.0 mmol) in MeOH/H$_2$O (60 mL, 3/1, v/v) was added LiOH (432 mg, 18.0 mmol) at room temperature, then the mixture was stirred and heated at 60 °C for 2 hours. After the reaction completed the mixture was evaporated to remove MeOH, then ice-water (20 mL) was added and the pH was adjusted to 3-4, then the suspension was filtered and the cake was washed by water and dried to give compound **7** (1.40 g, yield: 96%) as a white powder.

General Procedures for the Preparation of 8a-8n
A suspension of compound **7** (97 mg, 0.4 mmol), EDCI (96 mg, 0.5 mmol), HOBT (68 mg, 0.5 mmol) and DMAP (61 mg, 0.5 mmol) in DCM (3 mL) was stirred for 0.5 hour at room temperature, then a solution of amine (0.5 mmol) was added dropwise at room temperature and stirred overnight. After the reaction completed the mixture was extracted with dichloromethane, washed with brine. The organic layer was dried over Na_2SO_4 and concentrated under reduced pressure. The residue was purified by column chromatography using ethylacetate/hexane (1:19-1:5) to yield corresponding product **8a-8n**.

N,3-diphenyl-4H-thieno[3,2-b]pyrrole-5-carboxamide (8a)
Yellow solid, 112 mg, yield 88%. ^{1}H NMR (400 MHz, DMSO-d_6) δ 11.85 (s, 1H), 10.01 (s, 1H), 7.83 – 7.76 (m, 7.4 Hz, 4H), 7.69 (s, 1H), 7.49 (s, 2H), 7.40 – 7.36 (m, 4H), 7.09 (d, J = 6.5 Hz,, 1H). ^{13}C NMR (100 MHz, DMSO-d_6) δ 159.50, 139.59, 138.83, 134.08, 132.35, 129.28, 129.18, 127.85, 127.42, 127.28, 124.75, 124.59, 123.79, 120.45, 105.61. HRMS (E) calcd for $C_{19}H_{15}N_2OS^+$ [M+H]$^+$, 319.08996; found, 319.09079.

3-Phenyl-N-(thiazol-2-yl)-4H-thieno[3,2-b]pyrrole-5-carboxamide (8b)
Yellow solid, 84 mg, yield 64%. ^{1}H NMR (400 MHz, DMSO-d_6) δ 12.44 (s, 1H), 12.03 (s, 1H), 7.82 (d, J = 7.4 Hz, 2H), 7.78 (s, 1H), 7.58 (s, 1H), 7.55 (d, J = 3.5 Hz, 1H), 7.51 (t, J = 7.7 Hz, 2H), 7.39 (t, J = 7.3 Hz, 1H), 7.26 (d, J = 3.5 Hz, 1H). ^{13}C NMR (100 MHz, DMSO-d_6) δ 158.91, 158.51, 139.79, 138.22, 133.87, 130.00, 129.34, 127.96, 127.30, 127.10, 125.92, 125.15, 114.06, 107.71. HRMS (E) calcd for $C_{16}H_{12}N_3OS_2^+$ [M+H]$^+$, 326.04163; found, 326.04178.

(R)-3-phenyl-N-(1-phenylethyl)-4H-thieno[3,2-b]pyrrole-5-carboxamide (8c)
Yellow solid, 101 mg, yield 73%. ^{1}H NMR (400 MHz, DMSO-d_6) δ 11.60 (s, 1H), 8.55 (d, J = 8.0 Hz, 1H), 7.78 (d, J = 7.4, 2H), 7.62 (s, 1H), 7.47 (t, J = 7.6 Hz, 2H), 7.41 – 7.31 (m, 5H), 7.25 – 7.22 (m, 2H), 5.22 – 5.15 (m, 1H), 1.50 (d, J = 7.0 Hz, 3H). ^{13}C NMR (100 MHz, DMSO-d_6) δ 160.12, 145.27, 138.20, 134.22, 132.54, 129.31, 128.72, 127.79, 127.31, 127.21, 127.11, 126.55, 124.52, 123.85, 104.94, 48.43, 22.73. HRMS (E) calcd for $C_{21}H_{19}N_2OS^+$ [M+H]$^+$, 347.12126; found, 347.12115.

morpholino(3-phenyl-4H-thieno[3,2-b]pyrrol-5-yl)methanone (8d)
Light yellow solid, 70 mg, yield 56%. ^{1}H NMR (400 MHz, DMSO-d_6) δ 11.77 (s, 1H), 7.79 (d, J = 7.8 Hz, 2H), 7.63 (s, 1H), 7.45 (t, J = 7.5 Hz, 2H), 7.34 (t, J = 7.3 Hz, 1H), 6.84 (s, 1H), 3.71 (d, J = 3.3 Hz, 4H), 3.64 (d, J = 3.8 Hz, 4H). ^{13}C NMR (100 MHz, DMSO-d_6) δ 162.37, 137.57, 134.08, 130.40, 129.20, 127.72, 127.24, 127.09, 124.33, 123.23, 104.75, 66.74, 45.60. HRMS (E) calcd for $C_{17}H_{17}N_2O_2S^+$ [M+H]$^+$, 313.10052; found, 313.10086.

N-(3-fluorophenyl)-3-phenyl-4H-thieno[3,2-b]pyrrole-5-carboxamide (8e)
Yellow solid, 105 mg, yield 78%. ^{1}H NMR (400 MHz, DMSO-d_6) δ 11.90 (s, 1H), 10.18 (s, 1H), 7.83 – 7.76 (m, 3H), 7.71 (s, 1H), 7.53 – 7.47 (m, 3H), 7.42 – 7.36 (m, 3H), 6.91 (t, J = 7.9 Hz, 1H). ^{13}C NMR (100 MHz, DMSO-d_6) δ 162.60 (d, J = 241.4 Hz), 159.70, 141.44 (d, J = 11.1 Hz), 139.10, 134.02, 131.96, 130.78 (d, J = 10.1 Hz), 129.27, 127.87, 127.44, 127.28, 124.88 (d, J = 15.2 Hz), 116.04, 110.16 (d, J = 21.2 Hz), 107.17, 106.91 105.90. HRMS (E) calcd for $C_{19}H_{14}FN_2OS^+$ [M+H]$^+$, 337.08054; found, 337.08066.

N-(furan-2-ylmethyl)-3-phenyl-4H-thieno[3,2-b]pyrrole-5-carboxamide (8f)
Light yellow solid, 87 mg, yield 67%. ^{1}H NMR (400 MHz, DMSO-d_6) δ 11.63 (s, 1H), 8.71 (t, J = 5.6 Hz, 1H), 7.78 (d, J = 7.5 Hz, 2H), 7.64 (s, 1H), 7.60 (s, 1H), 7.47 (t, J = 7.6 Hz, 2H), 7.36 (t, J = 7.3 Hz, 1H), 7.18 (d, J = 1.1 Hz, 1H), 6.42 (t, J = 2.2 Hz, 1H), 6.32 (d, J = 3.0 Hz, 1H), 4.50 (d, J = 5.6 Hz, 2H). ^{13}C NMR (100 MHz, DMSO-d_6) δ 160.71, 152.87, 142.62, 138.28, 134.13, 132.24, 129.27, 127.79, 127.29, 127.17, 124.57, 123.96, 110.98, 107.54, 104.96, 35.96. HRMS (E) calcd for $C_{18}H_{15}N_2O_2S^+$ [M+H]$^+$, 323.08487; found, 323.08463.

N-(4-bromophenyl)-3-phenyl-4H-thieno[3,2-b]pyrrole-5-carboxamide (8g)
Light brown solid, 129 mg, yield 81%. ^{1}H NMR (400 MHz, DMSO-d_6) δ 11.88 (s, 1H), 10.13 (s, 1H), 7.82 (d, J = 7.4 Hz, 2H), 7.76 (d, J = 8.8 Hz, 2H), 7.70 (s, 1H), 7.55 (d, J = 8.8 Hz, 2H), 7.48 (t, J = 7.6 Hz, 2H), 7.41 – 7.36 (m, 2H). ^{13}C NMR (100 MHz, DMSO-d_6) δ 159.55, 139.03, 139.01, 134.03, 132.07, 131.99, 129.27, 127.86, 127.43, 127.28, 124.84, 124.80, 122.29, 115.37, 105.84. HRMS (E) calcd for $C_{19}H_{14}BrN_2OS^+$ [M+H]$^+$, 397.00047; found, 397.00107.

N-(3-bromophenyl)-3-phenyl-4H-thieno[3,2-b]pyrrole-5-carboxamide (8h)

Brown solid, 121 mg, yield 76%. ^{1}H NMR (400 MHz, DMSO-d_6) δ 11.89 (s, 1H), 10.14 (s, 1H), 8.09 (s, 1H), 7.82 (d, J = 7.4 Hz, 2H), 7.75 (d, J = 7.8 Hz, 1H), 7.71 (s, 1H), 7.49 (t, J = 7.3 Hz, 2H), 7.42 – 7.27 (m, 4H). ^{13}C NMR (100 MHz, DMSO-d_6) δ 159.63, 141.29, 139.11, 134.02, 131.90, 131.20, 129.28, 127.87, 127.43, 127.27, 126.29, 125.00, 124.84, 122.60, 121.96, 119.04, 105.95. HRMS (E) calcd for $C_{19}H_{14}BrN_2OS^+$ [M+H]$^+$, 397.00047; found, 397.00104.

3-Phenyl-N-(3-(trifluoromethyl)phenyl)-4H-thieno[3,2-b]pyrrole-5-carboxamide (8i)
Yellow solid, 107 mg, yield 69%. ^{1}H NMR (400 MHz, DMSO-d_6) δ 11.92 (s, 1H), 10.32 (s, 1H), 8.24 (s, 1H), 8.05 (d, J = 7.3 Hz, 1H), 7.83 (d, J = 6.6 Hz, 2H), 7.73 (s, 1H), 7.62 (d, J = 7.3 Hz, 1H), 7.51 – 7.38 (m, 5H). ^{13}C NMR (100 MHz, DMSO-d_6) δ 159.82, 140.48, 139.19, 134.00, 131.80, 130.44, 130.05, 129.73, 129.28, 127.88, 127.42, 127.26, 126.02, 125.10, 124.87, 123.78, 123.31, 122.39, 120.00, 119.96, 116.40, 116.35, 106.00. HRMS (E) calcd for $C_{20}H_{14}F_3N_2OS^+$ [M+H]$^+$, 387.07734; found, 387.07776.

(S)-3-phenyl-N-(1-phenylethyl)-4H-thieno[3,2-b]pyrrole-5-carboxamide (8j)
Yellow solid, 104 mg, yield 75%. ^{1}H NMR (400 MHz, DMSO-d_6) δ 11.60 (s, 1H), 8.55 (d, J = 7.9 Hz, 1H), 7.78 (d, J = 7.7 Hz, 2H), 7.62 (s, 1H), 7.47 (t, J = 7.6 Hz, 2H), 7.41 – 7.31 (m, 6H), 7.21 (s, 1H), 5.20 – 5.17 (m, 1H), 1.50 (d, J = 7.0 Hz, 3H). ^{13}C NMR (100 MHz, DMSO-d_6) δ 160.12, 145.28, 138.20, 134.22, 132.53, 129.31, 128.73, 127.79, 127.31, 127.21, 127.11, 126.55, 124.52, 123.86, 104.94, 48.43, 22.73. HRMS (E) calcd for $C_{21}H_{19}N_2OS^+$ [M+H]$^+$, 347.12126; found, 347.12115.

3-Phenyl-N-(thiophen-2-ylmethyl)-4H-thieno[3,2-b]pyrrole-5-carboxamide (8k)
Yellow solid, 90 mg, yield 66%. ^{1}H NMR (400 MHz, DMSO-d_6) δ 11.67 (s, 1H), 8.88 (s, 1H), 7.79 (d, J = 7.1 Hz, 2H), 7.64 (s, 1H), 7.48 – 7.36 (m, 4H), 7.18 (s, 1H), 7.05 (s, 1H), 6.97 (s, 1H), 4.67 (s, 2H). ^{13}C NMR (100 MHz, DMSO-d_6) δ 160.72, 143.19, 138.30, 134.10, 132.23, 129.25, 127.78, 127.31, 127.19, 127.14, 125.99, 125.59, 124.60, 123.98, 104.82, 37.72. HRMS (E) calcd for $C_{18}H_{15}N_2OS_2^+$ [M+H]$^+$, 339.06203; found, 339.06219.

N-cyclopropyl-3-phenyl-4H-thieno[3,2-b]pyrrole-5-carboxamide (8l)
Light yellow solid, 59 mg, yield 52%. ^{1}H NMR (400 MHz, DMSO-d_6) δδ 11.52 (s, 1H), 8.24 (d, J = 3.5 Hz, 1H), 7.78 (d, J = 7.3 Hz, 2H), 7.61 (s, 1H), 7.47 (t, J = 7.5 Hz, 2H), 7.37 (d, J = 7.3 Hz, 1H), 7.10 (s, 1H), 2.84 – 2.80 (m, 1H), 0.73 – 0.71 (m, 2H), 0.57 – 0.55 (m, 2H). ^{13}C NMR (100 MHz, DMSO-d_6) δ 162.07, 138.07, 134.17, 132.59, 129.26, 128.80, 127.77, 127.31, 124.50, 123.70, 104.45, 23.00, 6.33. HRMS (E) calcd for $C_{16}H_{15}N_2OS^+$ [M+H]$^+$, 283.08996; found, 283.08966.

N-(tert-butyl)-3-phenyl-4H-thieno[3,2-b]pyrrole-5-carboxamide (8m)
Light yellow solid, 77 mg, yield 64%. ^{1}H NMR (400 MHz, DMSO-d_6) δ 11.52 (s, 1H), 7.77 (d, J = 7.6 Hz, 2H), 7.59 (s, 2H), 7.48 (t, J = 7.5 Hz, 2H), 7.36 (t, J = 7.3 Hz, 1H), 7.13 (s, 1H), 1.40 (s, 9H). ^{13}C NMR (100 MHz, DMSO-d_6) δ 160.54, 137.87, 134.32, 133.52, 129.35, 127.78, 127.30, 127.21, 124.34, 123.48, 104.80, 51.25, 29.29. HRMS (E) calcd for $C_{17}H_{19}N_2OS^+$ [M+H]$^+$, 299.12126; found, 299.12106.

Tert-butyl 4-(3-phenyl-4H-thieno[3,2-b]pyrrole-5-carbonyl)piperazine-1-carboxylate (8n)
Light yellow solid, 92 mg, yield 56%. ^{1}H NMR (400 MHz, DMSO-d_6) δ 11.77 (s, 1H), 7.79 (d, J = 7.5 Hz, 2H), 7.63 (s, 1H), 7.45 (t, J = 7.6 Hz, 2H), 7.34 (d, J = 7.4 Hz, 1H), 6.86 (s, 1H), 3.70 (s, 4H), 3.42 (s, 4H), 1.42 (s, 9H). ^{13}C NMR (100 MHz, DMSO-d_6) δ 162.46, 154.30, 137.62, 134.53, 134.06, 130.46, 129.20, 127.72, 127.25, 127.10, 124.34, 123.30, 104.86, 79.66, 43.57, 28.52. HRMS (E) calcd for $C_{22}H_{26}N_3O_3S^+$ [M+H]$^+$, 412.16894; found, 412.16565.

N-(3,5-bis(trifluoromethyl)phenyl)-3-phenyl-4H-thieno[3,2-b]pyrrole-5-carboxamide (8o)
Light yellow solid, 133 mg, yield 73%. ^{1}H NMR (400 MHz, CDCl$_3$) δ 9.64 (s, 1H), 8.14 (s, 2H), 7.92 (s, 1H), 7.63 – 7.62 (m, 3H), 7.47 (t, J = 7.6 Hz, 2H), 7.40 – 7.35 (m, 2H), 7.05 (d, J = 1.9 Hz, 1H). ^{13}C NMR (100 MHz,

CDCl$_3$) δ 159.24, 139.82, 139.09, 133.84, 132.99, 132.66, 132.32, 131.99, 129.28, 129.11, 127.93, 127.12, 126.84, 126.52, 125.43, 125.24, 124.41, 121.69, 119.53, 117.54, 103.40. HRMS (E) calcd for $C_{21}H_{13}F_6N_2OS^+$ [M+H]$^+$, 455.06473; found, 455.06476.

4.3. Pharmacophore models, target prediction and molecular docking
The pharmacophore models, target prediction and molecular docking were all performed using Discovery Studio 2018R2 software package. Specifically, pharmacophore models were carried out by using pharmacophores module, which includes Edit and Cluster Features, Create Pharmacophore Automatically and Search, Screen and Profile tools. And target prediction was performed using Ligand Profiler protocol which contains a new pharmacophore database called "PharmaDB". Moreover, molecular docking was carried out by using pharmacophores module called "CDOCKER" protocol, which is an accurate molecular docking strategy based on CHARMm forcefield. The X-ray crystal structure of METAP2 (PDB code 1KQ0) complexed with ligand D-methionine was used as the reference receptor structure in the docking calculations, which was downloaded from the Protein Data Bank of RSCB.

4.4. Cell culture
Human colon cancer cells (HCT116, HT29) and normal colon cell (FHC) were obtained from the Nanjing Cobioer Co., Ltd (Jiangsu, China). Cells were grown in RPMI 1640 medium (Gibco, Beijing, China) containing 10% fetal bovine serum (Gibico, New York, NY, USA), penicillin (100U/mL, Gibco, Beijing, China), and streptomycin (100µg/mL, Gibco, Beijing, China). FHC was cultured in DMEM:F12 medium containing 10% FBS, 10ng/mL cholera toxin, 5µg/mL insulin, 5µg/mL transferrin and 100ng/mL hydrocortisone (Cobioer, Jiangsu, China). The cells were incubated at 37°C in a humidified air with 5% CO$_2$.

4.5. In vitro cytotoxicity assay
Cells were seeded in 96-well dish (1×10^4 cells/well). After 12 h of culture, the cells were treated with compouds at 20 µM or a series of concentration for 24, 48 and 72h, respectively. Upon completion of the incubation, stock 3-(4,5-dimethylthiazole)-2,5-diphenyltetrazolium bromide (MTT) dye solution (20µL) was added to each well and incubated for additional 4 h at 37°C. Then, 100µL dimethylformamide was added to solublilze the MTT formazan. The cell viability was obtained by measuring the optical density at 490 nm using a microplate reader (Cytation 5; BioTek, Winooski, VT, USA). The IC$_{50}$ values were determined by plotting the percentage viability versus concentration on a logarithmic graph and reading off the concentration at which 50% of cells remain viable relative to the DMSO control.

4.6. Colony formation assay
HCT116 and HT29 cells were trypsinized, counted, and seeded into 6-well dish at a density of xx cells/well. Cells were treated with compound **8i** at 5, 10, 20µM or DMSO for 12-14 day to allow for colony formation. After incubation, colonies were fixed and stained with 1% methylene blue in 50% ethanol at room temperature, and colonies consisting of more than 100 cells per well were counted by an inverted microscope (Olympus IX53; Olympus, Tokyo, Japan). Three independent experiments were carried out.

4.7. Annexin V-FITC apoptosis assay
HCT116 and HT29 cells were treated with compound **8i** at 0, 5, 10 and 20µM for 24h. Cells were stained with annexin V-FITC and PI (Beyotime Biotechnology Co. Ltd., Jiangsu, China) for 15min at room temperature in annexin V binding buffer, then analyzed using flow cytometry BD C6 (BD Biosciences, San Jose, CA). For each sample, data form 10,000 cells were recorded and the results were

interpreted with FlowJo software (Tree Star, FlowJo LLC, Ashland, OR).

4.8. Immunoblot analysis

HCT116 and HT29 cells were solubilized in RIPA lysis buffer containing protease and phosphatase inhibitor cocktails. Following centrifugation at 12,000g for 15min at 4°C, the concentration of protein in the supernatant was determined using a protein assay kit (Beyotime Biotechnology Co. Ltd., Jiangsu, China). Protein samples (20μg) were loaded into a SDS-polyscrylamide gel, separated by SDS-PAGE, transferred onto polyvinylidene fluoride (PVDF) membrane, and probed with specific antibodies against the following proteins: cleaved-caspase3, cleaved-caspase8, cleaved-caspase9, γH2AX, H2AX, Bax, Bcl2, PARP, p-Bad (all form CST, Danvers, MA). The blots were thoroughly rinsed and then incubated with an HRP-labeled species-matched secondary antibody for 1h at room temperature. Protein bands were detected by enhanced chemiluminescence (ECL, Thermo Fisher Scientific (China) Co., Ltd., Shanghai, China) and the signals were recorded using Tanon 5200 Luminescent Imaging Workstation (Tanon Science & Technology Co., Ltd., Shanghai, China) and software that helps to quantify the protein band intensities.

Acknowledgements

References

[1] A. Catalano, M. Romano, I. Robuffo, L. Strizzi, A. Procopio, *Am. J. Pathol.* **2001**, *159*, 721-731.

[2] A. Harada, K. Matsuzaki, A. Takeiri, M. Mishima, *Mutat. Res. Genet. Toxicol. Environ. Mutagen.* **2014**, *771*, 23-29.

[3] A. Iida, A. Yamaguchi, K. Hirose, *J. Surg. Oncol.* **2000**, *73*, 219-23.

[4] A. Ivashkevich, C. E. Redon, A. J. Nakamura, R. F. Martin, O. A. Martin, *Cancer Lett.* **2012**, *327*, 123-133.

[5] A. K. Bhattacharjee, J. W. Pomponio, S. A. Evans, D. Pervitsky, R. K. Gordon, *Bioorgan. Med. Chem.* **2013**, *21*, 2651-2662.

[6] A. M. Birch, P. W. Kenny, N. G. Oikonomakos, L. Otterbein, P. Schofield, P. R. O. Whittamore, D. P. Whalley, *Bioorg. Med. Chem. Lett.* **2007**, *17*, 394-399.

[7] C. Günther, E. Martini, N. Wittkopf, K. Amann, B. Weigmann, H. Neumann, M. J. Waldner, S. M. Hedrick, S. Tenzer, M. F. Neurath, C. Becker, *Nature* **2011**, *477*, 335-339.

[8] C. J. Gerry, S. L. Schreiber, *Nat. Rev. Drug Discov.* **2018**, *17*, 333-352.

[9] G. Badr, H. I. Gul, C. Yamali, A. A. M. Mohamed, B. M. Badr, M. Gul, A. Abo Markeb, N. Abo El-Maali, *Bioorg. Chem.* **2018**, *78*, 46-57.

[10] G. Dewson, T. Kratina, H. W. Sim, H. Puthalakath, J. M. Adams, P. M. Colman, R. M. Kluck, *Mol. Cell* **2008**, *30*, 369-380.

[11] H. Chen, M. Kanai, A. Inoue-Yamauchi, H. Tu, Y. Huang, D. Ren, H. Kim, S. Takeda, D. E. Reyna, P. M. Chan, Y. T. Ganesan, C. Liao, E. Gavathiotis, J. J. Hsieh, E. H. Cheng, *Nat. Cell Biol.* **2015**, *17*, 1270-1281.

[12] H. Chen, Y. Lee, S. Y. Huang, P. Shi, P. Hsu, C. Chang, *Oncotarget* **2018**, *9*, 13167-13180.

[13] I. Çoruh, Ö. Çevik, K. Yelekçi, T. Djikic, Ş. G. Küçükgüzel, *Arch. Pharm.* **2018**, *351*, 1700195.

[14] I. Endo, M. Gonen, A. C. Yopp, K. M. Dalal, Q. Zhou, D. Klimstra, M. D'Angelica, R. P. DeMatteo, Y. Fong, L. Schwartz, N. Kemeny, E. O'Reilly, G. K. Abou-Alfa, H. Shimada, L. H. Blumgart, W. R. Jarnagin, *Ann. Surg.* **2008**, *248*, 84-96.

[15] J. Boström, D. G. Brown, R. J. Young, G. M. Keserü, *Nat. Rev. Drug Discov.* **2018**, *17*, 922.

[16] J. D. Venable, H. Cai, W. Chai, C. A. Dvorak, C. A. Grice, J. A. Jablonowski, C. R. Shah, A. K. Kwok, K. S. Ly, B. Pio, J. Wei, P. J. Desai, W. Jiang, S. Nguyen, P. Ling, S. J. Wilson, P. J. Dunford, R. L. Thurmond, T. W. Lovenberg, L. Karlsson, N. I. Carruthers, J. P. Edwards, *J. Med. Chem.* **2005**, *48*, 8289-8298.

[17] J. L. Mauriz, J. Martín-Renedo, A. García-Palomo, M. J. Tuñón, J. González-Gallego, *Curr. Drug Targets* **2010**, *11*, 1439-1457.

[18] J. Parmentier, B. Portevin, R. M. Golsteyn, A. Pierré, J. Hickman, P. Gloanec, G. De Nanteuil, *Bioorg. Med. Chem. Lett.* **2009**, *19*, 841-844.

[19] J. Shen, L. Zeng, L. Pan, S. Yuan, M. Wu, X. Kong, *Oncol. Lett.* **2018**, *15*, 4557-4563.

[20] J. Sun, M. Li, S. Qian, F. Guo, X. Dang, X. Wang, Y. Xue, H. Zhu, *Bioorg. Med. Chem. Lett.* **2013**, *23*, 2876-2879.

[21] L. Sartori, C. Mercurio, F. Amigoni, A. Cappa, G. Fagá, R. Fattori, E. Legnaghi, G. Ciossani, A. Mattevi, G. Meroni, L. Moretti, V. Cecatiello, S. Pasqualato, A. Romussi, F. Thaler, P. Trifiró, M. Villa, S. Vultaggio, O. A. Botrugno, P. Dessanti, S. Minucci, E. Zagarrí, D. Carettoni, L. Iuzzolino, M. Varasi, P. Vianello, *J. Med. Chem.* **2017**, *60*, 1673-1692.

[22] M. A. Abu-Helalah, H. A. Alshraideh, M. D. Da Na, M. T. Al-Hanaqtah, A. Abuseif, K. Arqoob, A. Ajaj, *J. Gastrointest. Canc.* **2016**, *47*, 36-46.

[23] P. R. Adiyala, V. Tekumalla, I. B. Sayeed, V. L. Nayak, A. Nagarajan, M. A. Shareef, B. Nagaraju, A. Kamal, *Bioorg. Chem.* **2018**, *76*, 288-293.

[24] P. Selvakumar, A. Lakshmikuttyamma, U. Das, H. N. Pati, J. R. Dimmock, R. K. Sharma, *Mol. Cancer* **2009**, *8*, 65.

[25] P. Vianello, L. Sartori, F. Amigoni, A. Cappa, G. Fagá, R. Fattori, E. Legnaghi, G. Ciossani, A. Mattevi, G. Meroni, L. Moretti, V. Cecatiello, S. Pasqualato, A. Romussi, F. Thaler, P. Trifiró, M. Villa, O. A. Botrugno, P. Dessanti, S. Minucci, S. Vultaggio, E. Zagarrí, M. Varasi, C. Mercurio, *J. Med. Chem.* **2017**, *60*, 1693-1715.

[26] R. A. Gonzalez-Polo, P. Boya, A. L. Pauleau, A. Jalil, N. Larochette, S. Souquere, E. L. Eskelinen, G. Pierron, P. Saftig, G. Kroemer, *J. Cell Sci.* **2005**, *118*, 3091-102.

[27] R. Kumar, R. Bavi, M. G. Jo, V. Arulalapperumal, A. Baek, S. Rampogu, M. O. Kim, K. W. Lee, *Sci. Rep.-UK* **2017**, *7*, 10827.

[28] S. Kuriyama, T. Tsuji, T. Sakuma, T. Yamamoto, M. Tanaka, *Cell Death Discov.* **2018**, *4*, 11.

[29] S. N. L. Bennett, A. D. Campbell, A. Hancock, C. Johnstone, P. W. Kenny, A. Pickup, A. T. Plowright, N. Selmi, I. Simpson, A. Stocker, D. P. Whalley, P. R. O. Whittamore, *Bioorg. Med. Chem. Lett.* **2010**, *20*, 3511-3514.

[30] S. Tian, J. Wang, Y. Li, D. Li, L. Xu, T. Hou, *Adv. Drug Deliver. Rev.* **2015**, *86*, 2-10.

[31] T. Hirayama, M. Okaniwa, T. Imada, A. Ohashi, M. Ohori, K. Iwai, K. Mori, T. Kawamoto, A. Yokota, T. Tanaka, T. Ishikawa, *Bioorgan. Med. Chem.* **2013**, *21*, 5488-5502.

[32] T. Kanno, H. Endo, K. Takeuchi, Y. Morishita, M. Fukayama, S. Mori, *Lab. Invest.* **2002**, *82*, 893-901.

[33] T. Rodrigues, D. Reker, P. Schneider, G. Schneider, *Nat. Chem.* **2016**, *8*, 531-541.

[34] T. Rodrigues, D. Reker, P. Schneider, G. Schneider, *Nat. Chem.* **2016**, *8*, 531-541.

[35] Y. Zhang, Z. Li, Q. Min, A. Palida, Y. Zhang, R. Tang, L. Chen, H. Li, *Bioorg. Chem.* **2018**, *77*, 478-484.

[36] Z. Jia, H. H. Yang, Y. Liu, X. Wang, *Appl. Biochem. Biotech.* **2018**, *186*, 145-160.